Reflectance anisotropy spectroscopy of the Si(111)-(5 × 2)Au surface

C. H. Patterson, S. Banerjee, and J. F. McGilp
School of Physics, Trinity College Dublin, Dublin 2, Ireland
(Received 5 July 2016; revised manuscript received 20 September 2016; published 17 October 2016)

Hybrid DFT calculations of atomic structure, electronic band structure, and reflectance anisotropy (RA) are used to correlate atomic and electronic structures and optical transitions of eight structures for the Si(111)-(5 × 2)Au phase with Au coverage and Si adatom site occupancy. The structure recently proposed by Kwon and Kang (KK) [S. G. Kwon and M. H. Kang, Phys. Rev. Lett. **113**, 086101 (2014)] and strongly supported by surface x-ray diffraction [T. Shirasawa *et al.*, Phys. Rev. Lett. **113**, 165501 (2014)] is found to be the most stable in the Au coverage range from 0.6 to 0.8 ML. The band structure of the Si adatom covered (5 × 4) surface has a surface state whose dispersion and position agree very well with the prominent S_1 surface state observed in angle-resolved photoemission experiment. Reflectance anisotropy spectra in the energy range 0.5 to 5 eV for the eight surface structures show variations with Au and Si adatom coverage which can be explained in terms of filling of this surface state. The best agreement between predicted and measured RA spectra, which are sensitive to both Au atom and Si adatom coverage, is found for coverages from 0.7 to 0.75 ML Au, when the surface has regions where Si adatoms are absent and where there are sufficient adatoms to cause surface-state band filling, in equal parts. Surface formation energy calculations favor a coverage of 0.7-ML Au. The structures of the (5 × 2) KK and (6 × 6)Au phases on the Si(111) surface are compared and it is shown that the repeat unit of the KK phase also occurs in the (6 × 6) structure.

DOI: 10.1103/PhysRevB.94.165417

I. INTRODUCTION

Adsorption of Au on the Si(111) surface results in formation of (5 × 2), $(\sqrt{3}\times\sqrt{3})R30^\circ$, and (6 × 6) low-energy electron diffraction (LEED) patterns which were first observed over 40 years ago [1–3]. The $\sqrt{3}$ and (6 × 6) surface structures have been accepted for some time, but a consensus regarding the structure of the lower coverage (5 × 2) phase has only recently been established. The reported Au coverage for the (5 × 2) phase has varied from 0.4 [4] to 0.8 [5] monolayers (ML). A recent combined low-energy electron diffraction (LEED) and low-energy electron microscopy (LEEM) study found that the Au coverage is 0.65 ± 0.02 and 0.67 ± 0.01 [6]. A number of models have been proposed for the structure of the (5 × 2) phase based on scanning tunneling microscopy (STM) data [7–10], electron microscopy [4], and reflection high-energy electron diffraction RHEED) [11]. Several structural models have also been proposed on the basis of density functional theory (DFT) total energy methods [12–15].

The model proposed by Erwin, Barke, and Himpsel (EBH) [15] contains three parallel rows of Au atoms separated by single rows of Si honeycomb. The Au rows are connected by four Si atoms in the surface layer in the EBH model. The structure is similar to the honeycomb chain channel (HCC) structure in that an Si honeycomb separates metallic rows [16]. It is found in (3 × 1)-*M* phases at the Si(111) surface, where *M* is a monovalent metal atom such as an alkali metal or Ag [17]. Recently, Kwon and Kang (KK) [18] proposed a modified version of the EBH structure on the basis of DFT and computed scanning tunneling microscopy (STM) results. One Au atom was added to the Au rows per (5 × 2) unit cell, making the Au coverage equal to 0.7 ML. A recent surface x-ray diffraction (SXRD) study [19] found that the KK model reproduced in-plane and out-of-plane diffraction data.

ARPES measurements on the (5 × 2) phase reported either metallic [20,21], semiconducting [22,23], or mixed metallic and semiconducting [24] electronic structures. The local metallic or semiconducting electronic structure has been shown to depend on the presence or absence of Si adatoms on the Au chains [25,26]: addition of one Si adatom per $4a_0$ of the Au chains results in a gapped electronic structure with a (5 × 4) unit cell. a_0 is the Si(111) primitive lattice constant. Recent STM conductance measurements on metallic regions of various lengths ranging from $4a_0$ to $28a_0$ along the chain [27] have highlighted quantum well behavior induced by Si adatoms terminating metallic sections with no adatoms present.

The mixed metal-semiconductor behavior in this system has been explained on the basis of DFT calculations [18], where addition of one Si adatom per (5 × 4) unit cell induces a gap in a metallic state. Similar metal-semiconductor transitions have been observed by adding further Au to the metallic phase with a presumed 0.7-ML coverage and KK model structure [5,28] to yield a semiconducting phase with a proposed 0.8-ML Au coverage. In that case, the metal-semiconductor transition was probed using the disappearance of a low-energy plasmon in the infrared when the chains become semiconducting.

STM experiments have shown that a fraction of Si adatom sites are occupied [10,25–27,29–32] at the (5 × 2) surface. These atoms appear as "bright protrusions" which dominate the STM image where they are present. Si adatoms tend to aggregate along Au chains with a $4a_0$ period and regions containing aggregates of several adatoms are semiconducting with a local gap of around 0.6 eV [25]. Regions where there were no Si adatoms were found to be metallic.

In an attempt to quantify the behavior of Si adatoms at the (5 × 2) surface, Choi *et al.* [26] evaporated Si onto the preformed (5 × 2) phase at 423 K, after which treatment the adatom density was close to 100%, filling most of the remaining vacant sites in the KK structure with a $4a_0$ period along Au chains. Annealing this surface to 870 K reduced the adatom density to 48% and flashing the surface to 1173 K further reduced the adatom density to 37%. Results presented

for the stability of various adatom covered (5 × 2) phases are consistent with these STM observations. Adatoms bind to the (5 × 2) phase with about the same strength as in bulk Si and they open a band gap.

Here, we report hybrid DFT calculations of the relative energies, surface-state electronic structures, and optical excitations of the EBH (0.6-ML), KK (0.7-ML), and 0.8-ML structures with and without Si adatoms. We show that hybrid DFT calculations for a 50:50 combination of adatom-free and adatom-covered surfaces with 0.7-ML Au coverage are in excellent agreement with measured RA and ARPES spectra, as well as having the lowest surface formation energy of the range of surfaces tested. Dielectric functions of slabs are calculated with the electric vector parallel or perpendicular to Au chains and contact is made with experiment by using these dielectric functions to calculate the reflectance anisotropy (RA) spectrum for each surface structure and band filling. The RA response, which measures the difference of the surface optical response in two orthogonal directions normalized by the total response, is a severe test of structural models of this complex surface because of the small size of the signal (typically 1%) and the involvement of filled and empty electronic states and optical transition elements.

The remainder of this paper is arranged as follows: RA spectroscopy is described briefly; surface formation energy calculations of various (5 × 2) phases are compared; the evolution of the electronic band structure with Au and Si adatom coverage is compared to surface-state dispersion from ARPES experiment; RA spectra from hybrid DFT calculations and experiment are compared. Details of computational methods used, surface formation energy calculations, and a comparison between local structures in the (5 × 2) and (6 × 6) phases are given in the Supplemental Material [33].

II. REFLECTANCE ANISOTROPY

The reflectance anisotropy of a surface is defined by

$$\frac{\Delta r}{r} = 2\frac{r_x - r_y}{r_x + r_y}, \tag{1}$$

where r_α $(\alpha = x, y)$ is the complex reflection coefficient along a particular axis. The McIntyre-Aspnes three-layer model [34] is used to calculate the reflectivity of a surface from the susceptibility difference for a slab. Surface and bulk susceptibilities are calculated using the single-particle susceptibility expression in Eq. (5). The normalized change in reflectance, $\frac{\Delta R}{R}$, induced by a thin surface layer with the electric vector aligned along Cartesian x or y axes is

$$\frac{\Delta R_{x,y}}{R} = 2\,\mathrm{Re}\frac{\Delta r_{x,y}}{r} = 4kd\frac{\left(\Delta\chi^i_{xs}\chi^r_b - \Delta\chi^r_{xs}\chi^i_b\right)}{|\chi_b|^2}, \tag{2}$$

where the superscripts r and i indicate real and imaginary parts, k is the wave-vector magnitude of the incident light, and d is the surface-layer thickness. The frequency-dependent surface excess susceptibility [35] is defined by

$$\chi_{xs,\alpha}(\omega) = \chi_{s,\alpha}(\omega) - \chi_b(\omega). \tag{3}$$

The surface excess susceptibility difference for the two electric field orientations reduces to the difference in slab susceptibilities

$$\Delta\chi_{xs}(\omega) = \chi_{s,x}(\omega) - \chi_{s,y}(\omega). \tag{4}$$

The susceptibility of bulk χ_b or slab χ_s structures used in calculations is

$$\chi_\alpha(\omega) = \frac{2e^2}{m^2\epsilon_o\Omega\omega^2}\sum_{nn'\mathbf{k}}\frac{[f_o(E_{n\mathbf{k}}) - f_o(E_{n'\mathbf{k}})]|p^\alpha_{nn'\mathbf{k}}|^2}{\left(E_{nn'\mathbf{k}} - E - i\delta\right)}, \tag{5}$$

where f_o is a Fermi occupation factor, $p^\alpha_{nn'\mathbf{k}}$ is a momentum matrix element connecting states $n\mathbf{k}$ and $n'\mathbf{k}$ in the presence of a field along direction α, $E_{nn'\mathbf{k}}$ is the corresponding transition energy, and m, e, and Ω are the electron mass, charge, and unit-cell volume.

III. HYBRID DFT CALCULATIONS

All self-consistent field calculations were performed using the CRYSTAL program [36]. Both all-electron and pseudopotential calculations were performed. The basis set used for Si is described in Ref. [37] and the Si pseudopotential is described in Ref. [38]. Core electron basis functions from the basis set were omitted in pseudopotential calculations. The basis set and pseudopotential for Au is a version of the Hay-Wadt small core pseudopotential and basis [39] for Au modified by Weihrich and Anusca [40]. Calculations were performed without spin-orbit coupling; previous RA calculations for Au on stepped Si(111) surfaces [41] show that spin-orbit coupling makes only a small difference to RA spectra in this system.

Slabs used for surface electronic structure calculations contained two Si bilayers beneath the Si/Au top layer and were terminated by a pseudohydrogen layer underneath. Calculations were also performed on slabs terminated on both sides by an Si/Au layer with four Si bilayers to test convergence of these thin slabs. All atoms in the slab except the bottom layer of Si and the pseudohydrogen layer were allowed to relax during energy minimization calculations.

The hybrid DFT functional used in this work was a modified version of the B3LYP functional [42] in which the weight of Fock (exact) exchange was reduced from 0.2 to 0.05 in order to obtain improved agreement between the calculated and experimental dielectric functions of bulk Si. The weight of Fock exchange was adjusted so that the E_1 and E_2 peaks in the computed dielectric function of bulk Si agree as well as possible with experiment. Hence, no upwards shift of the empty state band structure is employed, as is sometimes done when an LDA approach (which underestimates the band gap) is used. Further details of this approach are given in Ref. [43].

Surface and bulk dielectric susceptibilities were calculated using the EXCITON code [44]. Integration over the Brillouin zone in dielectric function calculations was performed using an interpolation method. A 24 × 24 × 24 Monkhorst-Pack grid [45] was used for the Si bulk dielectric function calculations. Dielectric functions for slabs with (5 × 4) were calculated using 10 × 10 grids and an interpolation technique equivalent to the tetrahedron method for bulk solids. Tests using a 20 × 20 grid showed that optical spectra obtained with a 10 × 10 grid had converged.

Transitions which are responsible for specific peaks in surface dielectric functions are identified in band structure plots by placing an energy filter of width 0.2 eV on transitions

and inspecting magnitudes of optical matrix elements [Eq. (5)] across the entire Brillouin zone. The one-dimensional (1D) character of the electronic structure is also found in the variation of optical matrix elements with $\mathbf{k}_x$.

IV. RESULTS

A. Convex hull and surface formation energy

The surface energy per (1×1) surface unit cell is calculated using

$$E_{\text{surf}} = \frac{E_{\text{slab}} - N_{\text{Si}}E_{\text{Si}} - N_{\text{Au}}E_{\text{Au}} - 0.5N_{\text{H}}E_{\text{H}_2}}{N_{(1\times1)}}, \quad (6)$$

where E_{slab} is the DFT total energy for the slab representing the surface, N_i is the number of atoms of type i in the slab, and E_i is the energy per atom of Si, Au, or H in bulk Si, Au, or the H_2 molecule and $N_{(1\times1)}$ is the number of (1×1) cells in the slab. Results of surface energy calculations as a function of Au and Si adatom coverages are presented in a convex hull plot in the Supplemental Material [33].

Model structures for the (5×2) phase which are considered can be understood by beginning with the 0.6-ML Au EBH structure. This is shown in Fig. 1, top left, with four potential binding sites for Au atoms or Si adatoms highlighted as brown circles. The EBH structure is electron deficient and binds electron donor Au atoms and Si adatoms. The KK structure (Fig. 1, bottom left) is formed by adding an Au atom to every other vacant binding site and allowing the structure to relax. This system is also metallic and electron deficient. Addition of one Si adatom to every other remaining vacant binding site yields the structure shown in Fig. 1, top right. This structure is gapped. Instead of adding a Si adatom to the vacant sites in the KK structure, Au atoms can be added to the remaining vacant sites in a (5×4) unit cell so that the Au coverage is 0.75 or 0.8 ML (Fig. 1, bottom right).

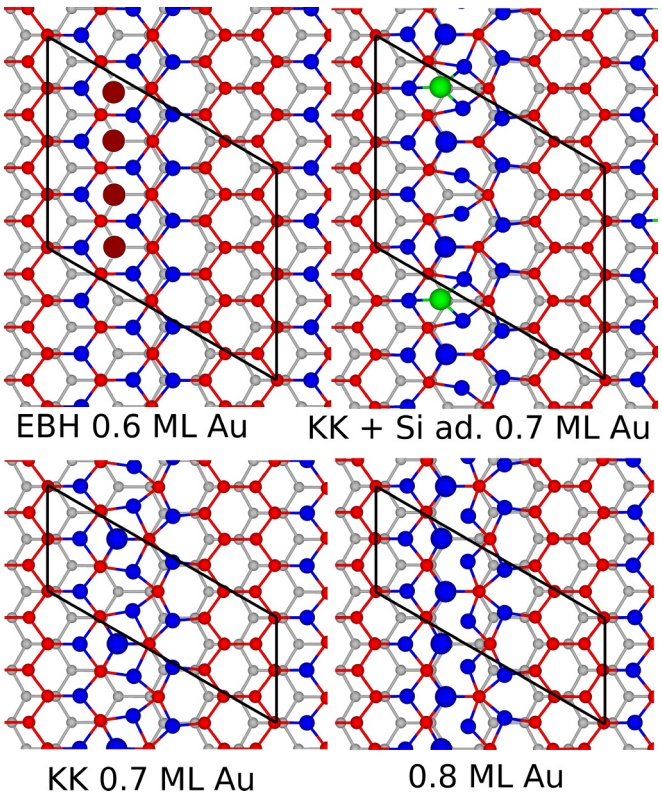

FIG. 1. Structures of EBH, KK, KK with Si adatom and 0.8-ML phases and available binding sites on the EBH structure. Vacant binding sites on EBH structure are shown as large brown circles. Au atoms (blue circles), top layer Si atoms (red circles), Si adatom (green circles), bulk Si bilayer (gray circles). Atoms added at binding sites are enlarged. These structures were originally proposed in Refs. [15,18,28].

The lowest-energy structures are the 0.7-ML KK structure with or without an Si adatom. Transfer of an Si atom from bulk Si to a surface site on the KK structure costs very little energy. The end-point structures in the convex hull plot at Au coverages of 0.6 and 0.8 ML are approximately 0.05 eV per (1×1) surface unit cell higher in energy than the 0.7-ML KK structure. Local structure elements such as $SiAu_4$ or $SiAu_5$ fragments in the topmost atomic layers of the KK and 0.8-ML structures in Fig. 1 also make up the structure of the (6×6) phase. Relationships between the structures of the (5×2) and (6×6) phases are discussed in the Supplemental Material [33].

B. Band structure and ARPES data

Interest in the (5×2) phase on Si(111) stems mainly from the quasi-1D metallic character of the Au chains, which have surface states with strong dispersion parallel to the chains and weak dispersion in the perpendicular direction. The most recent photoemission papers [23,24] on the (5×2) phase report similar band dispersions for photo-hole wave vectors parallel to Au chain directions. Variations in conductance measured by STM [27] can be explained by quantum confinement of electrons in metallic states by Si adatoms.

Surface Brillouin zones (SBZ) for (1×1), (5×1), (5×2), and (5×4) unit cells are shown in Fig. 2. The $\mathbf{k}_y$ direction is parallel to Au chains. Points where the Brillouin zone boundaries for the $(5 \times n)$ unit cells intersect the $\mathbf{k}_y$ axis are denoted $\overline{\mathbf{A}}_n$ points. Reciprocal lattice vectors for the surface unit cells are also shown in Fig. 2. All $\mathbf{b}_1$ vectors are parallel to $\mathbf{k}_x$ and $\mathbf{b}_2$ vectors for the (5×1) and (5×2) cells are nearly parallel to the $\mathbf{k}_y$ direction. Band dispersions in this work are plotted parallel to reciprocal lattice vectors (rather than $\mathbf{k}_y$) as the technique used to project wave-function amplitudes onto specific atomic sites requires wave functions on a regular grid defined by fractions of reciprocal lattice vectors. Surface-state dispersions perpendicular to Au chains are weak and so dispersions along $\mathbf{b}_2$ and $\overline{\Gamma\mathbf{M}}$ directions are very similar.

The strongest surface-state feature observed by ARPES [24] is a parabolic band whose minimum along $\overline{\Gamma\mathbf{M}}$ occurs at the $\overline{\mathbf{A}}_1$ point and has an occupied band width of about 1 eV. It is not observed at the $\overline{\Gamma}$ point of the SBZ, where it would coincide with bulk states. This state was denoted S_2 by Matsuda *et al.* [23] and "2" by McChesney *et al.* [24]. Here, it is referred to as S_2.

The EBH model structure with 0.6-ML Au coverage has a (5×1) unit cell and it must be electron doped in order to break symmetry to yield a (5×2) ground state [15]. In large period supercells such as the (5×4) cell there is much backfolding of

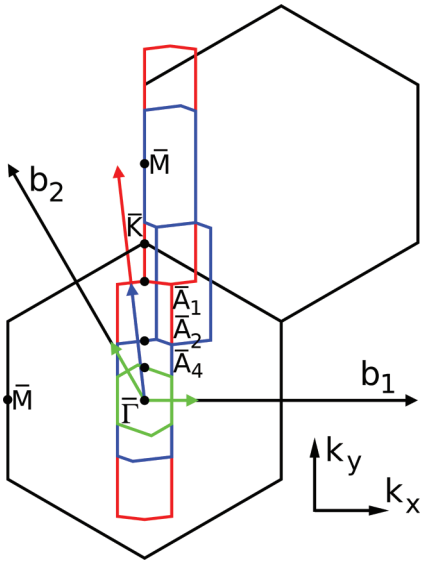

FIG. 2. Surface Brillouin zones and reciprocal lattice vectors for (1×1) (black), (5×1) (red), (5×2) (blue), and (5×4) (green) surface unit cells. Locations of $\overline{\mathbf{A}}_1$, $\overline{\mathbf{A}}_2$, and $\overline{\mathbf{A}}_4$ Brillouin zone points along the bulk $\overline{\Gamma}\overline{\mathbf{M}}$ direction are indicated by dots. $\mathbf{b}_1$ and $\mathbf{b}_2$ reciprocal lattice vectors for the (5×4) cell are labeled and correspond to labels used in Fig. 3.

bands. Photoemission experiments may not be able to observe backfolded energy bands because relevant Fourier components of the superlattice periodic potential may be weak. In a band structure calculation, backfolded bands are always present, even though some of them may not be observed in experiment. Hence, we plot the band structure of the (5×1) 0.6-ML phase in Fig. 3 (top panel). There are three Au atoms per cell in this structure and there are three partly filled bands mainly localized on Au chains in this case. The dispersion of the S_2 state is also plotted in the figure where it can be seen that the curvature of both the calculated and experimentally measured bands agrees well.

Addition of one Au atom to alternate (5×1) cells of the EBH structure yields the KK model structure with an Au coverage of 0.7 ML. The band structure of the KK model structure in a (5×2) cell is also shown in Fig. 3 (middle panel). There is one half-filled band in the SBZ, with a minimum at the $\overline{\Gamma}$ point which is localized mainly on Au chains. The bands around 1.3 eV above the valence band maximum are π^* states localized on the Si honeycomb chain. A state localized mainly on Au chains is found dispersing downwards from the $\overline{\mathbf{A}}_2$ point with a dispersion similar to the S_2 state.

Addition of one Si adatom to alternate (5×2) cells with the KK model structure yields a gapped state with a band gap of about 0.5 eV (Fig. 3, bottom panel). There are two filled subbands close to ϵ_F which result from backfolding of the single half-filled band of the adatom-free KK structure. The S_1 surface-state band dispersion is also plotted in this figure and it clearly matches well with the calculated band dispersion.

The variation of the band structure of the (5×4) Au system in Fig. 1 with addition of Au atoms to the four sites indicated in Fig. 1 and/or addition of Si adatoms is shown in Fig. 4. Dispersion from $\overline{\Gamma}$ to $\mathbf{b}_2/2$ (i.e., with a $\mathbf{k}_y$ component equal

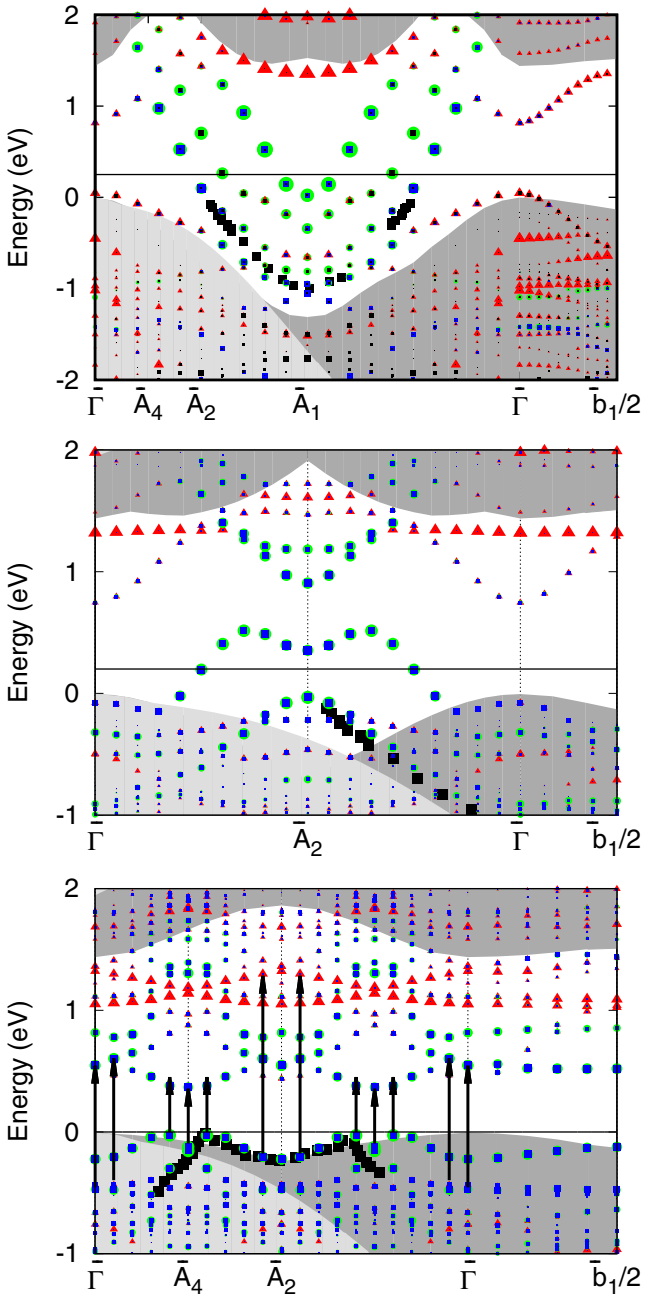

FIG. 3. Atom-projected electronic structures of EBH, KK, and adatom-covered KK model structures. Color coding of atom projections: red triangles, Si honeycomb; green circles, Si within Au chain; blue squares, Au. Hybrid DFT band dispersions are compared to dispersion of the S_1 and S_2 surface-state data of McChesney *et al.* [24] (black squares). Band structures are shown for one or two full periods of the reciprocal lattice along $\mathbf{b}_2$ lattice vectors (nearly parallel to Au chains) and for half a period of the reciprocal lattice along $\mathbf{b}_1$ lattice vectors. Points marked $\overline{\mathbf{A}}_n$ are $\mathbf{k}_y$ components of the $\mathbf{b}_2$ reciprocal lattice vectors. Energies are referenced to the bulk Si valence band maximum. (Top panel) EBH band structure in a (5×1) unit cell and experimental S_2 surface-state dispersion. (Middle panel) KK band structure in a (5×2) unit cell and experimental S_2 surface-state dispersion. (Bottom panel) KK structure with Si adatom band structure in a (5×4) unit cell and experimental S_1 surface-state dispersion. Transitions which contribute strongly to the RA spectrum are indicated by arrows.

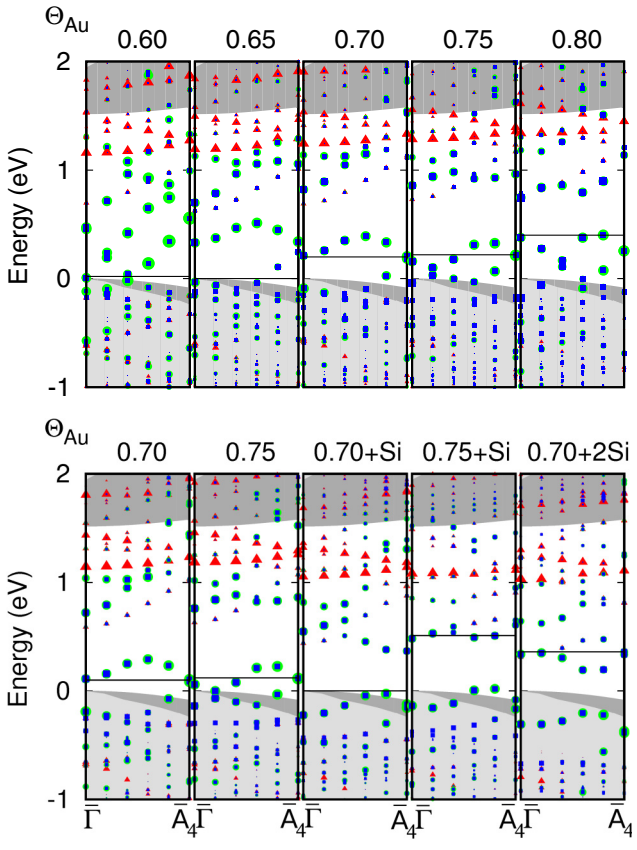

FIG. 4. Variation in electronic structure when Au atoms and/or Si adatoms are added to the vacant sites shown in Fig. 1. (Top panel) Atom-projected bands beginning with the 0.6-ML EBH structure with up to four added Au atoms (0.8-ML structure). The 0.70-ML structure is the adatom-free KK structure. The 0.80-ML case has a filled valence band and is gapped. (Lower panel) Atom-projected bands beginning with the 0.7-ML KK structure with added Au and/or Si adatoms. The 0.7-ML KK structure requires two electrons to achieve a filled surface-state band and the 0.7-ML KK structure with one Si adatom is gapped. ϵ_F is indicated by a solid horizontal line in each subpanel. Energies are referenced to the bulk Si valence band maximum. Atom projections are as follows: blue squares, Au; green circles, Si atoms within Au chains; red triangles, Si atoms in honeycomb.

to the $\bar{\mathbf{A}}_4$ point) is shown. The data shown in the top panel of Fig. 4 show that after one Au atom is added (mean Au coverage 0.65 ML), there are two subbands of the S_2 state in Fig. 3 which become completely filled as the coverage increases to 0.8 ML. Filling of the S_2 state by addition of Au atoms or Si adatoms correlates with relative stabilities of structures shown in Fig. 1. The lowest-energy structure is the 0.7-ML KK structure (Fig. 1, Supplemental Material [33]).

The lower panel in Fig. 4 shows how adding Au and Si adatoms affects band filling. Adjacent subpanels represent phases which have one more electron each step to the right. Addition of one Si adatom to every (5 × 4) cell is sufficient to fill the half-filled band just above the Fermi level (ϵ_F) in the 0.7-ML phase. Addition of one Au atom and one Si adatom (0.75 ML + Si) shifts ϵ_F into the lowest unoccupied surface band above the S_2 state and addition of two Si adatoms (0.70 ML + 2 Si) fills the first surface-state conduction band.

From these observations it is clear that Au behaves consistently as a one-electron donor and the Si adatom as a two-electron donor. The convex hull in Fig. 1 of the Supplemental Material [33] shows that the most stable phases are the KK 0.7-ML phase with or without an Si adatom. The 0.65-ML structure has the highest affinity for one more Au atom as it forms the 0.7-ML KK structure. Addition of an Si adatom to the KK structure from a bulk Si reservoir is almost cost neutral in energy. The 0.7-ML structure has a lower affinity for Au to form the 0.75-ML structure by about 1 eV. A detailed comparison to results of previous DFT calculations is given in the Supplemental Material [33].

C. Reflectance anisotropy spectra

In this section, RA spectra of the (5 × 2) phase from hybrid DFT calculations are compared with experimental data. RA spectra of systems which possess atomic chain structures, such as the π-bonded chain of the (2 × 1) reconstructed clean surface of Si(111) [46] or the Si(111)-(5 × 2)Au surface, are of particular interest since they directly show the anisotropy arising from chain structures and the 1D optical conductivity of the chains. The Si(111)-(2 × 1) clean surface reconstruction has a surface-state gap of 0.3 eV and exhibits a very large difference in reflectivity, parallel or perpendicular to atomic chains, when the photon energy in an RA experiment matches this gap. In data presented in this section, the reported RA is reflectivity parallel to Au chains minus reflectivity perpendicular to chains, normalized to the mean reflectivity. According to Eq. (2), in the photon energy region below the onset of bulk Si transitions around 3 eV, a positive RA signal implies that the imaginary part of the surface dielectric function parallel to Au chains is greater than that perpendicular to chains.

Figure 5 shows evolution of RA spectra for the 0.6-ML EBH structure with up to four Au atoms added per (5 × 4) cell. An earlier DFT-LDA study of RA spectra [48], which was published before the KK structure had been proposed [18] and strongly supported by SXRD [19], used the EBH structure with and without Si adatoms. Subsequent experimental work has proposed that Au coverages up to 0.8 ML in the (5 × 2) phase are possible [5]. Here, we compare RA spectra to experiment for all structures and coverages described above. Changes in the RA spectrum induced by sequentially adding Au atoms to the EBH structure are reported first and then the changes induced by adding Si adatoms. Since as-prepared Si(111)-(5 × 2)Au surfaces contain a mixture of adatom-covered and adatom-free regions, RA spectra for mixed surfaces are also compared to experimental data.

RA spectra shown in the two panels of Fig. 5 arise from transitions between the bands shown in the two panels of Fig. 4. There is a one-to-one correspondence between band structures and RA spectra in these figures. As noted above, experimental data in this work were obtained from a vicinal Si(111) surface offcut by 2° towards [11$\bar{2}$]. The sample displayed a largely monodomain (5 × 2) LEED pattern. The Au coverage is not known precisely as the preparation procedure involves depositing Au on the clean sample held at 700 K until the RA response is maximized [49]. Similar data were reported

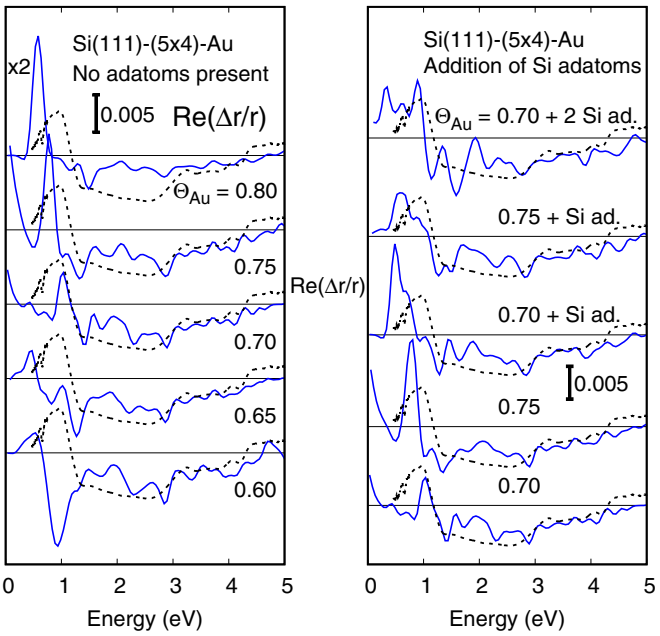

FIG. 5. Variation in RA spectrum when Au atoms and/or Si adatoms are added to vacant sites in the EBH structure shown in Fig. 1. Dashed curves are experimental data from Si(111)-(5 × 2)Au grown on a Si(111) surface offcut by 2° towards [11$\bar{2}$] recorded at room temperature [47]. Solid blue curves were calculated using hybrid DFT. (Left panel) RA spectra for the EBH structure (0.60 ML) with up to four added Au atoms. The 0.70-ML case is the adatom-free KK structure. The 0.80-ML case is gapped. (Right panel) RA spectra for the KK structure (0.70 ML) with added Au and/or Si adatoms. The 0.70 ML + Si adatom structure is gapped. RA spectra in these panels correspond directly with the band structures shown in the two panels in Fig. 4. RA spectra from hybrid DFT calculations have been scaled by $\frac{1}{2}$, except for the 0.80-ML Au spectrum, which has been scaled by $\frac{1}{4}$ relative to the scale represented by the 0.005 bar.

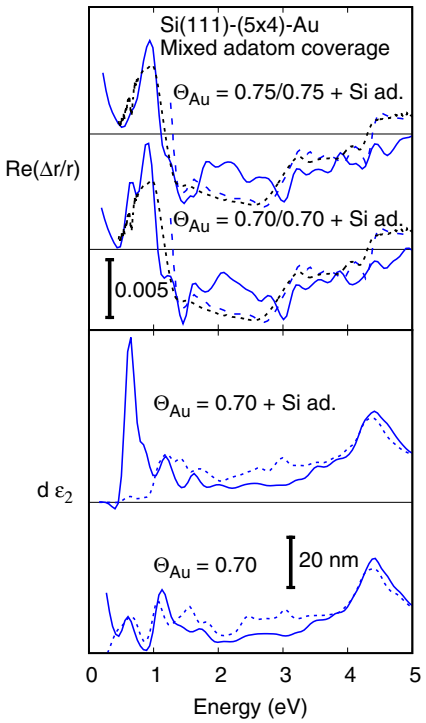

FIG. 6. (Upper panel) RA spectra generated by 50:50 weighted sums of spectra for surfaces with coverages of 0.70- or 0.75-ML Au, with and without one Si adatom per 5 × 4 cell. A bar representing 0.005 RAS units is shown in each panel. RA spectra from hybrid DFT calculations have been scaled by $\frac{1}{2}$ relative to the scale represented by the bar and shifted to higher energy by 0.15 eV. Experimental data from Ref. [47] (recorded at room temperature) and redrawn from Supplemental Material of Ref. [28] (recorded at 20 K) are shown as dotted and dashed lines, respectively. (Lower panel) Surface dielectric functions times slab thickness d for the 0.70-ML Au surface with and without a Si adatom. The electric vector is either parallel to Au chains (solid curves) or perpendicular to them (dotted curves).

previously in Ref. [50] and the contribution to the RA signal from steps was deduced to be small.

The lower panel of Fig. 6 shows surface dielectric functions for the 0.7-ML KK structure, with and without one Si adatom per (5 × 4) cell. Below the onset for bulk Si transitions, the RA spectrum shape is approximately proportional to the difference in these dielectric functions. There are three peaks in the surface dielectric function for the adatom-covered surface below 2 eV when the electric vector is aligned parallel to Au chains. The strong peak around 0.5 eV in the surface dielectric function produces the strong positive peak in the RA spectrum (Fig. 5). This peak is much reduced in intensity when the adatom is removed, leaving a peak at just over 1.0 eV as the strongest feature in the surface dielectric function and resulting in an upward shift in RA peak position when no adatom is present. Vertical arrows in the bottom panel of Fig. 3 show the electronic transitions which are largely responsible for these three peaks. The intense peak around 0.5 eV is caused by transitions between surface states around the $\overline{\mathbf{A}}_4$ point. The occupied surface state in this transition becomes unoccupied when the Si adatom is removed, which explains why the corresponding peak in the RA spectrum is nearly extinguished in that case. The peak around 1 eV is caused by transitions between occupied surface states and the two lowest-lying empty surface states close to the $\overline{\Gamma}$ point. The initial and final states in this transition do not change occupation and the corresponding peak in the surface dielectric function is unchanged when a Si adatom is added or removed. The peak around 1.5 eV is caused by transitions around the $\overline{\mathbf{A}}_2$ point between the highest occupied surface state and surface states higher in the conduction band.

The main differences between experimental and calculated RA spectra are in the range 2 to 3 eV where experiment shows a flat region with a negative slope and the calculated spectra have a negative slope but are not as deep as the experimental data. The RA spectra are negative in this region as the surface dielectric function for transitions induced with the electric vector perpendicular to Au chains is stronger than those induced with the vector parallel to Au chains. There are no strong features in the calculated surface dielectric function for either electric vector orientation in this region and the cause of the difference is unknown.

It is immediately clear from Fig. 5 that RA spectra for this surface present a strong test of surface structure models. Coverage changes of 5% have a large effect on the hybrid

DFT RA curves owing to band filling. The RA spectrum for the 0.6-ML EBH structure in a (5×4) unit cell is shown at the bottom of the left panel of Fig. 5. It contains a strong dip around 1 eV, while experimental data show a peak here. Band structures presented in Fig. 4 show that there is a large change in electronic structure when the (5×1) periodicity of the EBH structure is broken by adding one Au atom every fourth vacant site on the Au chain. The two subbands which are $\frac{1}{2}$ filled in the 0.7-ML KK structure appear with $\frac{1}{4}$ filling. The RA spectrum changes considerably on going from 0.6 to 0.65 ML (Fig. 5) with a reduction in the dip at 1 eV seen for the EBH structure.

The Si(111)-(5×2)Au system is metallic in the 0.7-ML KK structure in regions which are free of Si adatoms, but the strongest optical transitions occur around 1 eV. Band folding of the $\frac{1}{2}$ filled band containing ϵ_F in the (5×2) cell KK phase leads to two $\frac{1}{2}$ filled subbands in the (5×4) cell. Weak transitions between these subbands lead to RAS features below 1 eV. The main peak and dip in the RA spectrum occur around 1 eV. As the subbands fill on adding two more Au atoms per (5×4) cell, the peak at 1 eV shifts to lower energy and strengthens considerably. In the gapped phase at 0.8-ML Au, the subbands are full and strong transitions to the lowest unoccupied surface states lead to a two times more intense peak at 0.5 eV.

The panel on the right in Fig. 5 shows the effect of adding Si adatoms and introducing electrons into the lowest unoccupied surface states of the 0.7-ML KK structure. One valence electron is added to the (5×4) cell in each upwards step from the bottom to the top of the panel. The middle RA curve for the 0.7-ML phase with one Si adatom is gapped. It resembles the RA spectrum for the gapped 0.8-ML phase with no adatoms in the left panel. Since Si adatoms act as two electron donors in this system, adding a Si adatom to the 0.75-ML phase introduces one electron into the surface-state conduction band and adding two Si adatoms to the 0.7-ML phase introduces two electrons to the conduction band. There is an accompanying weakening of the peak around 0.5 eV in the gapped phases, presumably because transitions to the bottom of the surface-state conduction band are now not possible.

Si(111)-(5×2)Au surfaces prepared in experiment [9,25,26] typically have an Si adatom coverage of 0.5 adatoms per (5×4) cell (0.025 ML) according to STM measurements. RA spectra presented in Fig. 5 are either for surfaces with no adatoms or a coverage of 0.05 ML. The upper panel of Fig. 6 compares RA spectra for 50:50 mixed regions with (0.05-ML Si adatoms) and without Si adatoms for Au coverages of 0.7 and 0.75 ML. These spectra were generated from weighted sum spectra. Spectra for surfaces with single phases have significantly narrower lines than these weighted sums of spectra. However, since there is a shift in peak position when Si adatoms are adsorbed, the weighted spectra have line shapes very similar to the experimental spectra shown in Figs. 5 and 6.

It is worth noting that there may be a small peak on the left of the main experimental peak, which is reproduced in the weighted spectrum for 0.7-ML Au. There is also a weak dip feature above 1 eV before the experimental spectrum flattens out between 1.5 and 3 eV. Hybrid DFT calculations generally show more structure than experiment, and may predict more intense and sharper peaks than those observed in experiment at room temperature. An example of this can be seen in features related to surface-state transitions in the Si(111)-(3×1)Ag surface [17]. The weak dip around 1.3 eV in experiment for the (5×2) surface is reproduced in both calculated spectra in Fig. 6. Smearing of features in experimental RA spectra may be caused by, e.g., phonons and short excited surface-state lifetimes in RA measurements. This dip feature becomes stronger at low temperature (20 K, Ref. [28] Supplemental Material) and is discussed further in Sec. V.

V. DISCUSSION

Calculations presented in the previous section on the 1D chains of the (5×2) system predict a ground state with the KK structure and one half-filled band per (5×2) cell. This band becomes filled when one Au single electron donor is added per (5×2) cell to form the 0.8-ML gapped phase [5]. Alternatively, the KK system can become gapped if one Si adatom two-electron donor is added per (5×4) cell [18]. Surface formation energy calculations presented in the Supplemental Material [33] favor the latter 0.7-ML KK phase.

The interplay of atomic and electronic structure and their effect on the optical properties of the system probed via RA spectroscopy are discussed here. Electron counting in the (5×2) and related $\sqrt{3}$ and Si(111)-(3×1)Ag [17] systems gives an explanation for the number of electrons required for a gapped state at the Si(111)/Au or Ag surfaces.

Electron counting for Si atoms in the Si honeycomb structure of the Si(111)-(3×1)Li or Ag systems [17] [which is very similar to the honeycomb structure in Si(111)-(5×2)Au] shows that each Si atom at each edge of the honeycomb chain requires one electron from a donor for saturation. This extra electron leaves the edge Si atoms with an electron lone pair. We assume the same electron counting rule in the honeycomb moiety of the (5×2) phase.

Electron counting for Si atoms in the $\sqrt{3}$ and (5×2) phases suggests that the preferred electron count for top-layer Si atoms in the Au chains of the (5×2) phase is four. The KK structure contains seven Au atoms and four Si atoms in Au chains per (5×2) cell. One valence electron per Si within the Au chain is needed to form a covalent bond with the Si atom in the bulk bilayer directly beneath it. Excluding this electron from the electron count, Si atoms contribute three electrons each and each Au contributes one electron to bonding in Au chains or to the Si honeycomb, giving a total of 19 electrons in the top layer for *in-plane* bonding. Four of these are transferred to the Si atoms at edges of honeycomb chains, leaving 15 electrons per (5×2) cell in the Au chains. In a non-spin-polarized state, this yields one half-filled band per unit cell. Addition of one more electron yields an electron count of 16, or four in-plane bonding electrons per top-layer Si in Au chains.

A similar ideal number of bonding electrons is also found in the $\sqrt{3}$ phase [51]. The $\sqrt{3}$ cell contains three Au and three Si atoms in the top layer. Each Au behaves as a one-electron donor to top-layer Si atoms, resulting in four valence electrons per Si (again excluding electrons binding those Si atoms to the bilayer beneath). In this case, however, the system is not gapped with four electrons per Si as there is a strongly dispersing surface

state which is partly filled and has been clearly identified by ARPES experiments [52]. In that case, extra Au atoms are incorporated in interstitial sites to form the $\alpha\sqrt{3}-$ Au phase (Ref. [51] and references within).

A Mulliken population analysis of the EBH structure in this work shows 4.64 and 4.77 electrons on the two types of Si atom in Au chains, 4.36 electrons at honeycomb edges and 3.94 electrons per Si in honeycomb interiors. These values exceed the value of four electrons per Si mentioned above as the Mulliken population analysis includes the electron pair bonding the top layer to the bilayer beneath. When Au atoms are added to the EBH structure to form the KK structure, the average populations of Si atoms in Au chains rise by 0.32 electrons, while other Si populations are essentially unchanged, demonstrating that doped charge is accumulated in the Au chains and not the honeycomb.

The electronic band structure obtained using hybrid DFT methods used in this work is essentially the same as has been reported previously for the KK structure [5,18] and the 0.8-ML structure [5] in (5×2) cells. There is a half-filled band with a minimum at the $\overline{\Gamma}$ point and a maximum close to the $\overline{\mathbf{A}}_2$ point of the SBZ. When calculated in a (5×4) cell, band folding produces two subbands from this single band, which fill progressively as further Au or Si adatoms are added. There is very good agreement between the S_1 state dispersion from ARPES experiment in Ref. [24] and the filled surface-state band dispersion in Fig. 3, bottom panel, and also S_2 state dispersion and Au localized states in Fig. 3, top and middle panels, which disperse downwards from the $\overline{\mathbf{A}}_2$ point of the SBZ. A more detailed comparison of band structures is given in the Supplemental Material, Sec. C.

RA spectra in Fig. 5 change markedly in shape on going from the EBH to the KK structures. As surface-state bands fill, by adding one Si adatom to the KK structure in a (5×4) cell or by increasing the Au coverage to 0.8-ML Au, the RA spectrum narrows into a sharp peak around 0.5 eV which increases in strength. This is likely to be because of the increased density of states in the valence band with band filling and transitions occurring across the surface-state band gap. The linewidth of the filled surface-state band RA peak is significantly less than the experimental RA spectrum in Figs. 5 and 6. STM experiments [10,25,26] have shown that the (5×2) surface which forms under the usual preparation conditions contains about 0.025-ML Si adatoms [or one adatom per two (5×4) cells]. Furthermore, STS experiments [25] have shown that Si adatoms cluster along Au chains with a $4a_0$ period to yield gapped areas and that areas from which Si adatoms are missing are conducting. It is therefore expected that RA measurements performed under these conditions will yield spectra which are a combination of RA spectra from both types of region. This hypothesis seems to be supported by the very good agreement between the experimental and calculated RA line shapes in Fig. 6, which are linear combinations of spectra from adatom-covered and adatom-free surfaces.

Changes in RA spectra induced by adding extra Au to a (5×2) surface which exhibited an RA spectrum similar to the experimental data shown in Figs. 5 and 6 are consistent with band filling, according to calculated RA spectra in these figures. Figures S3 and S4 in Ref. [28] (and reproduced here in Fig. 6) show a dip around 1.4 eV which is also present in experimental data shown in Figs. 5 and 6, which were recorded at room temperature. It becomes much more pronounced at 20 K [28]. This dip disappears when extra Au is added in the experiment, and in our calculations as the surface-state band becomes filled, either by adding Si adatoms or Au.

As-prepared (5×2) surfaces normally have an adatom coverage of 0.025 ML, equivalent to one Si adatom per two (5×4) cells. The maximum Si adatom coverage is 0.05 ML [29]. There are insufficient vacant adsorption sites to permit a coverage of 0.8-ML Au when Si adatoms are present. Filling each vacant adsorption site shown in Fig. 1 would yield a maximum Au coverage of 0.75 ML, when the Si adatom coverage is 0.05 ML. In that case, the lowest-energy surface-state conduction band would contain one electron. The upper part of Fig. 6 shows a 50:50 weighted sum of RA spectra for the 0.75-ML Au surface with no adatoms and with one adatom per (5×4) cell. It is also in very good agreement with room-temperature experimental data, and it also contains the more pronounced dip found at 1.4 eV when the spectrum is recorded at 20 K [28].

VI. SUMMARY

Si(111)-(5×2)Au surface atomic and electronic structures, and optical transitions, have been studied using a hybrid DFT method. A recent determination of the atomic structure of this surface [18,19] has made it possible to compare surface-state optical transitions observed via reflectance anisotropy spectra to results of hybrid DFT calculations. Predicted RA spectra evolve with band filling of a surface state as Au or Si adatoms are added to (5×4) unit cells. The best agreement with experimental data is obtained for surfaces with 0.70- or 0.75-ML Au and a combination of regions where Si adatoms are absent or present with a coverage of about 0.05 ML (as observed in STM experiments). Calculations of the convex hull with Au coverages ranging from 0.6 to 0.8 ML and adatom coverages ranging from 0 to 0.05 ML, show that the most stable phases are the 0.7-ML KK structure, with or without a Si adatom. Surface-state dispersions for the KK structure with an Si adatom coverage of 0.05 ML are in very good agreement with those obtained from ARPES experiments [23,24]. Combining RA spectroscopy and hybrid DFT calculations produces a powerful tool for probing anisotropic surface structures, due to the high sensitivity of RA spectra to surface atomic and electronic structure.

ACKNOWLEDGMENTS

This work was supported by Science Foundation Ireland under Grant No. 11/RFP/PHY/3047. Calculations were performed on the Kelvin cluster, maintained by the Trinity Centre for High Performance Computing, funded through grants from the Irish Higher Education Authority through its PRTLI programme and the Fionn cluster, maintained by the Irish Centre for High End Computing and funded by Science Foundation Ireland. The authors wish to thank L. Marks for advice on calculating the convex hull in the Supplemental Material [33].

[1] H. E. Bishop and J. C. Riviére, J. Phys. D: Appl. Phys. **2**, 1635 (1969).
[2] H. Lipson and K. E. Singer, J. Phys. C: Solid State Phys. **7**, 12 (1974).
[3] G. L. Lay, Surf. Sci. **132**, 169 (1983).
[4] L. D. Marks and R. Plass, Phys. Rev. Lett. **75**, 2172 (1995).
[5] F. Hötzel, K. Seino, C. Huck, O. Skibbe, F. Bechstedt, and A. Pucci, Nano Lett. **15**, 4155 (2015).
[6] J. Kautz, M. W. Copel, M. S. Gordon, R. M. Tromp, and S. J. van der Molen, Phys. Rev. B **89**, 035416 (2014).
[7] T. Hasegawa, K. Takata, S. Hosaka, and S. Hosoki, J. Vac. Sci. Technol. A **8**, 241 (1990).
[8] A. A. Baski, J. Nogami, and C. F. Quate, Phys. Rev. B **41**, 10247 (1990).
[9] J. D. O'Mahony, C. H. Patterson, J. F. McGilp, F. M. Liebsle, P. Weightman, and C. F. J. Flipse, Surf. Sci. **277**, L57 (1992).
[10] J. D. O'Mahony, J. F. McGilp, C. F. J. Flipse, P. Weightman, and F. M. Leibsle, Phys. Rev. B **49**, 2527 (1994).
[11] T. Abukawa and Y. Nishigaya, Phys. Rev. Lett. **110**, 036102 (2013).
[12] S. Erwin, Phys. Rev. Lett. **91**, 206101 (2003).
[13] S. Riikonen and D. Sánchez-Portal, Phys. Rev. B **71**, 235423 (2005).
[14] C.-Y. Ren, S.-F. Tsay, and F.-C. Chuang, Phys. Rev. B **76**, 075414 (2007).
[15] S. C. Erwin, I. Barke, and F. J. Himpsel, Phys. Rev. B **80**, 155409 (2009).
[16] C. Collazo-Davila, D. Grozea, and L. D. Marks, Phys. Rev. Lett. **80**, 1678 (1998).
[17] S. Jorgji, J. F. McGilp, and C. H. Patterson, Phys. Rev. B **87**, 195304 (2013).
[18] S. G. Kwon and M. H. Kang, Phys. Rev. Lett. **113**, 086101 (2014).
[19] T. Shirasawa, W. Voegeli, T. Nojima, Y. Iwasawa, Y. Yamaguchi, and T. Takahashi, Phys. Rev. Lett. **113**, 165501 (2014).
[20] I. R. Collins, J. T. Moran, P. T. Andrews, R. Cosso, J. D. O'Mahony, J. F. McGilp, and G. Margaritondo, Surf. Sci. **325**, 45 (1995).
[21] R. Losio, K. N. Altmann, and F. J. Himpsel, Phys. Rev. Lett. **85**, 808 (2000).
[22] K. N. Altmann, J. N. Crain, A. Kirakosian, J.-L. Lin, D. Y. Petrovykh, F. J. Himpsel, and R. Losio, Phys. Rev. B **64**, 035406 (2001).
[23] I. Matsuda, M. Hengsberger, F. Baumberger, T. Greber, H. W. Yeom, and J. Osterwalder, Phys. Rev. B **68**, 195319 (2003).
[24] J. L. McChesney, J. N. Crain, V. Pérez-Dieste, F. Zheng, M. C. Gallagher, M. Bissen, C. Gundelach, and F. J. Himpsel, Phys. Rev. B **70**, 195430 (2004).
[25] H. S. Yoon, S. J. Park, J. E. Lee, C. N. Whang, and I. W. Lyo, Phys. Rev. Lett. **92**, 096801 (2004).
[26] W. H. Choi, P. G. Kang, K. D. Ryang, and H. W. Yeom, Phys. Rev. Lett. **100**, 126801 (2008).
[27] E. H. Do and H. W. Yeom, Phys. Rev. Lett. **115**, 266803 (2015).
[28] F. Hötzel, K. Seino, S. Chandola, E. Speiser, N. Esser, F. Bechstedt, and A. Pucci, J. Phys. Chem. Lett. **6**, 3615 (2015).
[29] A. Kirakosian, J. N. Crain, J.-L. Lin, J. L. McChesney, D. Y. Petrovykh, F. J. Himpsel, and R. Bennewitz, Surf. Sci. **532-535**, 928 (2003).
[30] A. Stepniak, P. Nita, M. Krawiec, and M. Jalochowski, Phys. Rev. B **80**, 125430 (2009).
[31] A. Stepniak, M. Krawiec, G. Zawadzki, and M. Jalochowski, J. Phys.: Condens. Matter **24**, 095002 (2012).
[32] I. Barke, S. Polei, V. v. Oeynhausen, and K.-H. Meiwes-Broer, Phys. Rev. Lett. **109**, 066801 (2012).
[33] See Supplemental Material at http://link.aps.org/supplemental/10.1103/PhysRevB.94.165417 for surface formation energy calculations for the (5×2) phase in (5×4) unit cells with Au coverages of 0.60, 0.65, 0.70, 0.75, and 0.80 ML Au, with or without Si adatoms. Results of these calculations are compared to previous DFT formation energy results in the literature. Finally, a comparison of local structure units in the (5×2) and (6×6) phases is given.
[34] J. D. E. McIntyre and D. E. Aspnes, Surf. Sci. **24**, 417 (1971).
[35] M. K. Kelly, S. Zoller, and M. Cardona, Surf. Sci. **285**, 282 (1993).
[36] R. Dovesi, V. R. Saunders, C. Roetti, R. Orlando, C. M. Zicovich-Wilson, F. Pascale, B. Civalleri, K. Doll, N. M. Harrison, I. Bush *et al.*, Crystal09 User's Manual, University of Torino, Torino, 2009.
[37] F. Pascale, M. Catti, A. Damin, R. Orlando, V. Saunders, and R. Dovesi, J. Phys. Chem. B **109**, 18522 (2005).
[38] A. Bergner, M. Dolg, W. Kuechle, H. Stoll, and H. Preuss, Mol. Phys. **80**, 1431 (1993).
[39] P. J. Hay and W. R. Wadt, J. Chem. Phys. **82**, 299 (1985).
[40] R. Weihrich and I. Anusca, Z. Anorg. Allg. Chem. **632**, 335 (2006).
[41] C. Hogan, N. McAlinden, and J. F. McGilp, Phys. Status Solidi B **249**, 1095 (2012).
[42] A. D. Becke, J. Chem. Phys. **98**, 5648 (1993).
[43] S. Banerjee, J. F. McGilp, and C. H. Patterson, Phys. Status Solidi B **252**, 78 (2015).
[44] C. H. Patterson, Mol. Phys. **108**, 3181 (2010).
[45] H. Monkhorst and J. D. Pack, Phys. Rev. B **13**, 5188 (1976).
[46] C. H. Patterson, S. Banerjee, and J. F. McGilp, Phys. Rev. B **84**, 155314 (2011).
[47] N. McAlinden, Ph.D. thesis, Trinity College, Dublin, 2011.
[48] C. Hogan, E. Ferraro, N. McAlinden, and J. F. McGilp, Phys. Rev. Lett. **111**, 087401 (2013).
[49] N. McAlinden and J. F. McGilp, J. Phys.: Condens. Matter **21**, 474208 (2009).
[50] N. McAlinden and J. F. McGilp, Europhys. Lett. **92**, 67008 (2010).
[51] C. H. Patterson, J. Phys.: Condens. Matter **27**, 475001 (2015).
[52] L. V. Bondarenko, D. V. Gruznev, A. A. Yakovlev, A. Y. Tupchaya, D. Usachov, O. Vilkov, A. Fedorov, D. V. Vyalikh, S. V. Eremeev, E. V. Chulkov *et al.*, Sci. Rep. **3**, 01826 (2013).